Journal of Materials Chemistry A

Accepted Manuscript

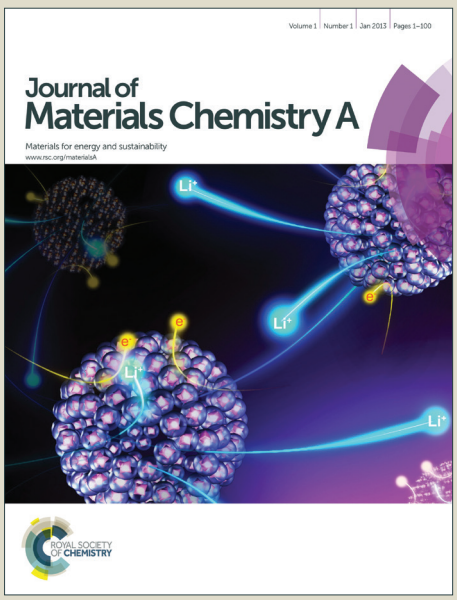

ROYAL SOCIETY OF CHEMISTRY

www.rsc.org/materialsA

Journal of Materials Chemistry A RSCPublishing

ARTICLE

High Photocurrent in Oligo-thienylenevinylene-Based Small Molecule Solar Cells with 4.9% Solar-to-Electrical Energy Conversion.

Cite this: DOI: 10.1039/x0xx00000x

Received 00th January 2012,
Accepted 00th January 2012

DOI: 10.1039/x0xx00000x

www.rsc.org/

Núria F. Montcada,[a+] Rocío Domínguez,[b+] Beatriz Pelado,[b] Pilar de la Cruz,[b] Emilio Palomares[*a,c] and Fernando Langa[*b]

A set of five novel oligo-thienylenevinylene organic molecules have been synthesized and characterized for use as electron donor moieties in bulk-heterojunction solution-processed organic solar cells combined with $PC_{71}BM$ as an electron acceptor. The results show a broad range of solar-to-electrical conversion efficiencies, with values up to 4.9% achieved with a photocurrent value as high as 12 mA cm^{-2} under standard measurement conditions. Moreover, another aim of this study was to determine the main limiting processes that control the final performance parameters of these devices. Photo-induced charge transfer measurements, such as charge extraction (CE), Transient Photo-Voltage (TPV) and mobility measurements, were carried out in order to determine the main loss mechanisms and to correlate them with the electron donor molecular design.

Introduction

Fundamental research into organic solar cells based on solution-processed semiconductor molecules (so called Small Molecule Organic Solar Cells, smOSC) has attracted considerable attention due to the increase in the device efficiency upon sun-simulated irradiation. Novel synthetic strategies for the electron donor molecules along with the optimization of film nanomorphology have led to new 'champion' cells with published efficiencies close to 10% for single junction devices.[1]

The use of small molecules is a growing field because they have several advantages over semiconductor polymers, such as reproducible synthesis, high degree of purity and ease of scale-up among others.[2-5] However, several questions remain unanswered, for example the molecular design and its correlation with the final device performance.[6-10]

We present here a complete study of a novel set of small molecules built around a 3,4-ethylenedioxythiophene (EDOT) group and based on the previously published work on **smL01**.[11] These molecules all have a high-symmetry Acceptor-π-Donor-π-Acceptor (A-π-D-π-A) molecular architecture in order to favour solid-state packing.[12] On the one hand, we consider this approach to be one of the most promising strategies for molecular band-gap tuning as an effective interaction between intercalating electron-rich donors and electron-deficient acceptors reduces the optical band-gap and certainly tunes the HOMO and LUMO energy levels to maximize the intermolecular charge transfer. On the other hand, the presence of the π-bridging groups, branched thienylenevinylenes in our case, improves intra-molecular π-delocalization. Moreover, the carrier mobility in the organic blend is one of the major limiting processes for smOSC-based device efficiencies and this is generally reflected in their low fill factors (FF).[8,13] Thus, selection of an appropriate acceptor moiety is also very important because of the role that this plays within the electron donor molecule to improve hole mobility. Furthermore, it is important that the acceptor is strong enough to pull the maximum number of electrons from the donor, thus increasing the absorption capability of the donor moiety. However, the main drawback of this strategy is that choosing an acceptor that is too strong may also decrease the hole mobility or shift the LUMO, thus impeding charge dissociation.[14,15]

In the work described here we analysed and compared all of the aspects discussed above and evaluated their effects on the final device characteristics, with the results compared with those obtained in our previous[11] study using **smL01**. The effect of increasing the number of thienylenevinylene units, two thienylenevinylene (**smL02**) and three thienylenevinylene (**smL03**) units per side, was studied in order to determine the effect of the intramolecular π-delocalization and the effect on the absorption capability of the donor moiety. In addition, the removal of one of the alkyl chains of the thiophene (**smL04** and **smL06**) was studied to provide information about the real role of these pendant groups both

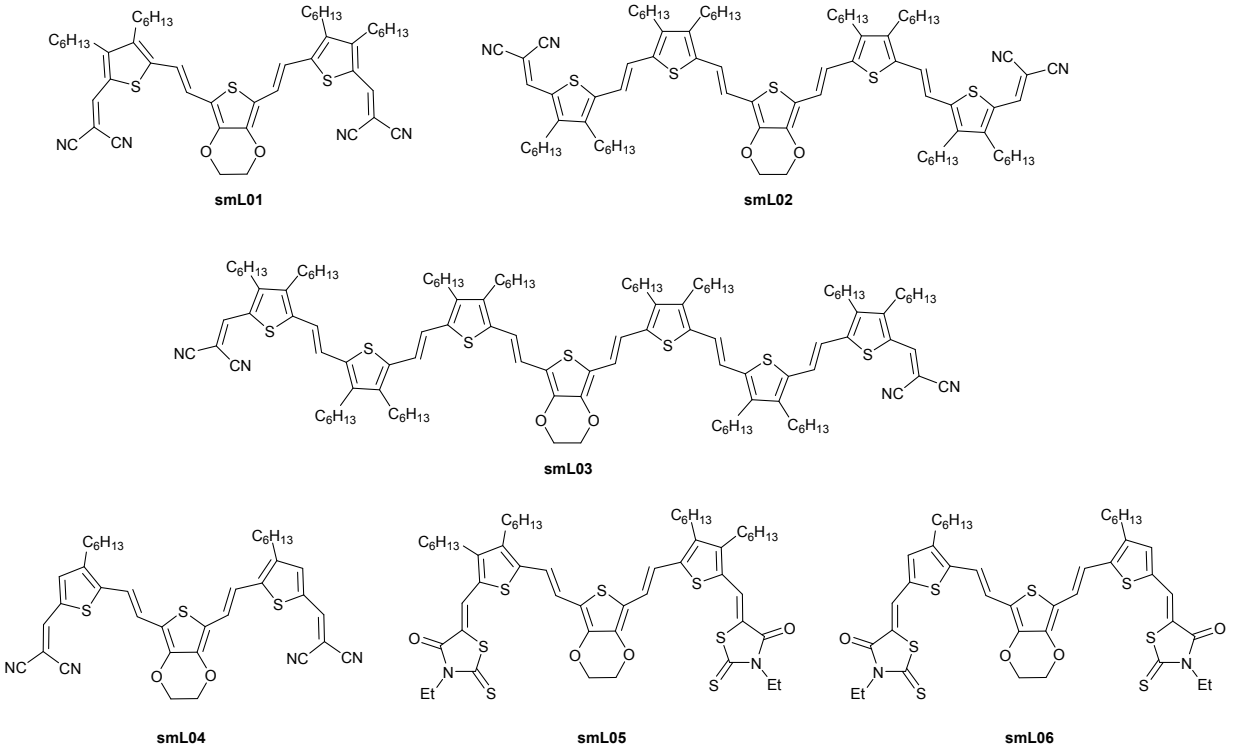

Scheme 1 Chemical structures for **smL01–06**.

morphologically and energetically. Finally, a direct comparison was made between two different acceptor moieties, dicyanovinylene (DCV) and rhodanine (Rho) (**smL04** and **smL06**), with the latter being a less electrophilic compound. This strategy was investigated with the aim of determining the effect of the strength of the acceptor moiety and the repercussions that this has on the transport properties within the molecule. The molecular structures of the molecules used in this study are shown in Scheme 1.

Results and discussion

Synthesis, photochemical and electrochemical characterization of the molecules.

The synthesis of **smL04** and **smL06** started from bis-aldehyde **5a**, whereas **smL05** was prepared from bis-aldehyde **5b** and the synthesis of **smL02** and **smL03** was described elsewhere.[16] Bis-aldehyde **5a** was synthesized from 2-formyl-3-hexylthiophene **1** by quantitative reduction with sodium borohydride, followed by zinc bromide-mediated Michaelis–Arbuzov reaction of **2** to give phosphonate **3** (84% yield, Scheme 2). Horner–Emmons reaction of **3** with 2,5-bisformyl-3,4-ethylenedioxythiophene afforded **4** in 36% yield. Finally, Vilsmeier formylation of **4** yielded **5a** in 73% yield.

The synthetic approach to **smL04**, **smL05** and **smL06** is depicted in Scheme 3. Knoevenagel condensation of **5a** with malononitrile provided the dicyanovinylene (DCV)-capped derivative **smL04** in 70% yield and Knoevenagel condensation of **5a–b** with 3-ethylrhodanine gave **smL05** and **smL06** (69% and 62% yields, respectively).

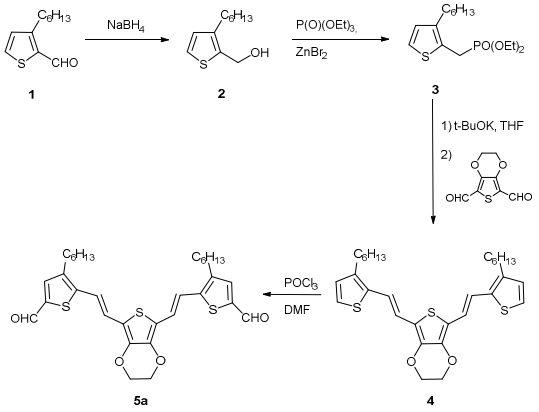

Scheme 2 Synthetic pathway to **5a**.

All compounds were characterized by ^{1}H-NMR, ^{13}C-NMR, FT-IR and MALDI-TOF MS analysis to confirm the structures (see SI). In all cases, the *E* configuration was confirmed for the double bond by coupling constants in the order of 15 Hz.

Thermogravimetric analysis (TGA) results suggest that **smL04–06** have good stability, with decomposition temperatures (Td) above 320 ºC under an N_2 atmosphere (see SI, Figs. S24–26).

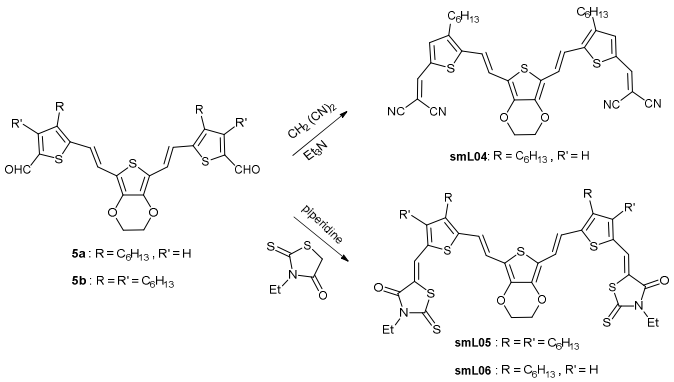

Scheme 3 Synthetic pathway to **smL04–06**.

The absorption spectra of oligomers **smL01–06** measured in dichloromethane are shown in Fig. 1 and the data are summarized in Table 1. Transformation of the formyl moieties to dicyanovinylene groups in **smL01** and **smL04** led to a red-shift in the lowest energy absorption band to 618 nm and 611 nm, respectively. These bands are ascribed to a charge transfer transition due to the donor–acceptor interactions between the electron-rich inner part of the molecule (EDOT) and the electron-deficient peripheral part (dicyanovinylene moieties). On the other hand, replacement of the aldehyde groups with 3-ethylrhodanine led to a stronger red-shift (to 632 nm and 622 nm, respectively) for derivatives **smL05** and **smL06** and this is due to the extension of the conjugation. For compounds **smL02** and **smL03**, the increased length of the π-conjugated system yielded red-shifted absorptions with maxima at 646 nm and 647 nm, respectively, with a tail on the absorption at around 800 nm. It should be noted that the extension of the conjugation from **smL02** to **smL03** caused a red-shift of only 1 nm, indicating that the saturation limit had been reached.

All of these new compounds have low optical band-gaps, in the range 1.75–1.87 eV, with the lower values corresponding to the compounds with a higher HOMO, **smL02** and **smL03**, due to the extension of the conjugation.

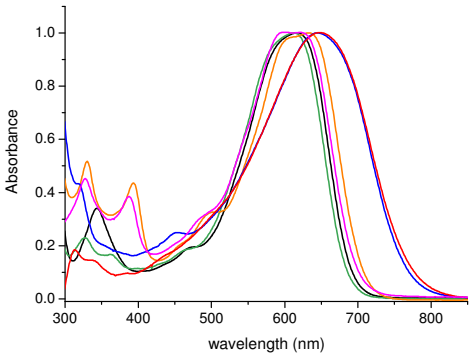

Fig. 1 Normalized UV-vis spectra of **smL01** (—), **smL02** (—), **smL03** (—), **smL04** (—), **smL05** (—) and **smL06** (—) in CH_2Cl_2 ([ ] ≈ 2.5 10^{-6} M).

The oxidation potentials of **smL01–06** were investigated by Osteryoung Square Wave Voltammetry (OSWV) in *o*-dichlorobenzene/acetonitrile (4:1) solutions under argon (Table 1, Figs. S29–S34). This study was carried out to determine the energy levels of the HOMOs of the newly synthesized materials as the alignment of the HOMO values is very important to achieve a high open circuit voltage (V_{oc}) as this energy is closely related to the energy difference between the HOMO of an electron-donating material and the LUMO of an electron-accepting material. Compounds **smL01** and **smL04**, which have dicyanovinylene groups as terminal acceptor units, show the lowest HOMO values and they should therefore give the highest V_{oc} values in PV devices (*vide infra*).

Table 1 Optical and electrochemical parameters of compounds **smL01–06**

Molecule	λ_{abs} (nm)	log ε	λ_{em} [a] (nm)	E^1_{ox} [b] (V)	$E_{0\text{-}0}$ [c] (eV)	HOMO [d] (eV)	LUMO [e] (eV)
smL01	618	4.87	709	0.50	1.87	–5.60	–3.73
smL02	646	4.85	796	0.16	1.76	–5.26	–3.50
smL03	647	5.21	784	- 0.07	1.80	–5.03	–3.23
smL04	611	4.89	704	0.52	1.88	–5.62	–3.74
smL05	632	4.86	727	0.31	1.82	–5.41	–3.59
smL06	622	4.97	722	0.31	1.84	–5.41	–3.57

[a] Excitation at maximum wavelength. [b] OSWV (Osteryoung square wave voltammetry) value. [c] Optical value. [d] Calculated according to the equation: $E_{HOMO} = -5.1 - E_{ox1(OSWV)}$. [e] Calculated according to the equation: $E_{LUMO} = E_{HOMO} + E_{0,0}$ (eV).[17]

Theoretical Calculations.

Quantum chemical calculations were carried out in an effort to gain an insight into the geometrical, electronic and optical properties of **smL01–06**. The ground-state geometries of these molecules were fully optimized by density functional theory (DFT) at the B3LYP 6-31G* level *in vacuo* with Gaussian 03W. The optimized geometries and the electron density distributions of the HOMO and LUMO of **smL01–06** are shown in Fig. S35. In all cases, the calculated ground-state geometries reveal an almost planar conformation of the conjugated system[18] (dihedral angles ≈ 1–2°), with the acceptor unit, dicyanovinylene or 3-ethylrhodanine, *cis* to the thiophene S-atom. This planar conformation must favour π-π stacking between the molecular backbones. Two possible conformations were calculated for the molecules that contained 3-ethylrhodanine as the acceptor unit (**smL05** and **smL06**), namely **smL05**-A and **smL05**-B (Scheme S1). Conformation **smL05**-A, in which the two sulphur atoms face one another, was more stable than **smL05**-B – a finding that is consistent with results for related compounds.[19] It should be noted that in **smL05**-A the distance between the two sulphur atoms is 3.27 Å, i.e., lower than the sum of the Van der Waals radii (3.70 Å), thus suggesting the existence of through space non-bonding interactions between them.

It is very useful to determine the electronic distribution of the HOMO and LUMO levels as they provide information about the photovoltaic properties of the molecules. The electron density of the HOMO for all molecules is mainly distributed on the EDOT central unit and the oligothienylenevinylene backbone, whereas the density for the LUMO is mainly localized on the terminal acceptor groups and the adjacent thienylenevinylene units. The calculated band gap is around 2 eV for the molecules with three thiophene rings (**smL01** and **smL04-06**) and the band gaps are significantly lower for **smL02** and **smL03** (ΔE = 1.63 and 1.50 eV, respectively, Fig. S37) due to the more extended conjugation in these systems. The values obtained are in reasonably good agreement with the experimental values.

Organic film characterization.

The molecules were deposited on a substrate using conditions determined from the optimization studies (See SI). The absorbance in the film was measured for each pristine molecule (See SI) and in blends with fullerene. The light harvesting efficiencies (LHE) were calculated using Equation 1 and the results are shown in Fig. 2.

Equation 1 $$LHE = 1 - 10^{-abs(\lambda)}$$

Compound **smL01** showed the highest LHE peak (65%) at λ = 690 nm; the other molecules were deposited under the same processing conditions. In the cases of **smL02** and **smL03** it is clear that the addition of each thienylenevinylene group favours broader and more red-shifted absorption spectra (bathochromic shift). For **smL04** the LHE is slightly below that of **smL01** and a shift towards longer wavelengths was also observed. The Rho-based molecules **smL05** and **smL06** present lower LHE values than **smL01-04** and this indicates that the presence of the Rho substituents leads to weaker CT bands.

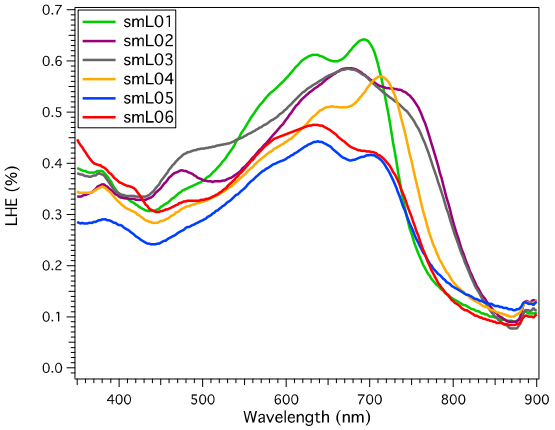

Fig. 2 Light harvesting efficiency (LHE) for all **smL** molecules blended with $PC_{71}BM$. The films were 75 nm thick.

Characterization of organic solar cells.

Complete devices were fabricated using the optimized conditions and the devices were characterized by IV measurements. The results for the optimized cell of each set are shown in Fig. 3 and their main performance parameters are shown in Table 2.

The results obtained in this study of **smL01** are in good agreement with those obtained in our previous work, although in this work a new batch of **smL01** was synthesized. Compounds **smL02** and **smL03** present lower photocurrent values as the number of thienylenevinylenes in the backbone increases. This finding led us to consider a direct relationship between the number of thiophenes and a significant increase in the recombination of free charges, as discussed later in this work. Taking into account the results of previous studies, the presence of the alkyl chains on both sides of the molecule disfavours the required π-π interaction, thus impeding inter-chain charge hopping.[3, 13, 19]

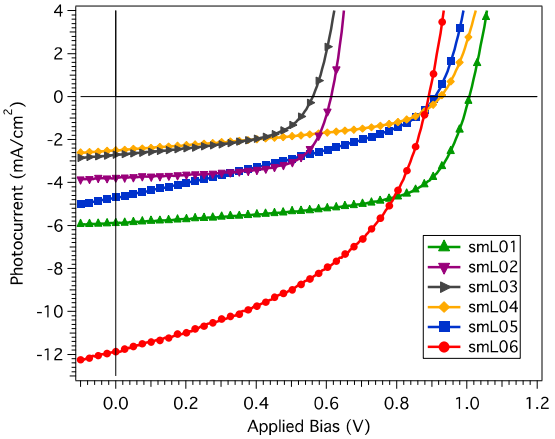

Fig. 3 Photocurrent *vs* voltage (IV) curves for optimized **smL:PC$_{71}$BM** solar cells at 1 sun (sun simulated 100 mWcm^{-2} light intensity).

Moreover, the lower V_{oc} observed for **smL02** and **smL03** compared to **smL01** is due to the differences in the HOMO energy level. Additionally, the EQE measurements shown in Fig. 4 show a marked reduction in the IPCE spectra, a situation consistent with the measured photocurrent from the IV curves.

Table 2 Main performance parameters for optimized organic solar cells using **smL:PC$_{71}$BM** bulk-heterojunction 75 nm thick films

Device	J_{sc} (mA/cm^2)	V_{oc} (mV)	FF (%)	PCE (%)
smL01	5.85	1000	63.70	3.7
smL02	3.78	613	66.43	1.5
smL03	2.70	562	52.61	0.8
smL04	2.50	924	45.43	1.1
smL05	4.70	910	34.91	1.5
smL06	11.98	890	45.69	4.9

J_{sc} = Short-circuit current density; V_{oc} = Open-circuit voltage; FF = Fill factor; PCE = Photo-current efficiency. Devices have an active area of 9 mm^2.

In the case of **smL04** removal of hexyl groups from the molecular structure clearly has a negative effect on the photocurrent and, moreover, the decrease in V_{oc} is also related to this subtle change in the molecular structure.

The DCV acceptor group was replaced by a Rho in **smL05** and **smL06**. In **smL05** devices a reduction of the photocurrent accompanied by a steep reduction of the FF and also a slight decrease in the V_{oc} can be observed. A proportion of this V_{oc} leakage occurs due to the difference in the HOMO energy level position (–5.41 eV). The poorer FF caused by variations in the nanomorphology of the active layer indicates that Rho does not provide domains that are as crystalline as those in DCV-based molecules. This is due to variations in intramolecular polarity[13] that also have an impact on the final photocurrent. Indeed, differential scanning calorimetry analysis (**DSC**) revealed that the molecules with 3-ethylrhodanine as the acceptor unit, such as **smL06**, have amorphous properties, while those molecules with dicyanovinylene as the acceptor unit, such as **smL01**, exhibit crystalline properties (see SI, Figs. S27–S28).

The reduction in this photocurrent starts with the limitation of the LHE, as discussed previously, because fewer photons can be absorbed using the same thickness and also fewer photons are finally converted to external current, as shown in Fig. 4.

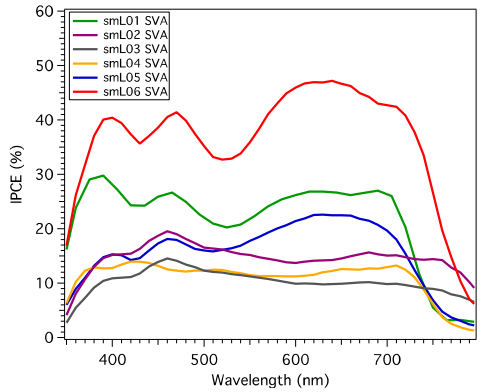

Fig. 4 Incident Photon-to-Current Efficiency (IPCE) spectrum for the devices measured in Fig. 2.

On the other hand, the use of the same optimized fabrication conditions with **smL06** led to a PCE of nearly 5% and the highest photo-current (12 mA cm^{-2}). These results indicate better self-organization compared to **smL05**. Taking into account the external quantum efficiency results shown in Fig. 4, **smL06** shows the highest incident photon-to-current efficiency. The CE results for all **smL** complete devices are shown in Fig. 5. The geometric capacitance was calculated using Equation 2.

Equation 2 $$C_g = \frac{\varepsilon_0 \varepsilon_r A}{d}$$

Where C_g is the geometrical capacitance, which is related to the charge that the organic thin film has because is 'sandwiched' between two metal electrodes. ε_r is the dielectric constant for the organic material, which is estimated to be ≈ 3 for organic materials, ε_0 is the dielectric constant (8.854×10^{-12} F m^{-1}), A is the solar cell area (9 mm^2) and d is the film thickness (75 nm).

Considering that the solar cell area for all devices is equal and that the film thickness is also very similar in the solar cells as measured by an AFM type profilometer (75 nm), the Cg value was calculated to be 65 nF/cm^2.

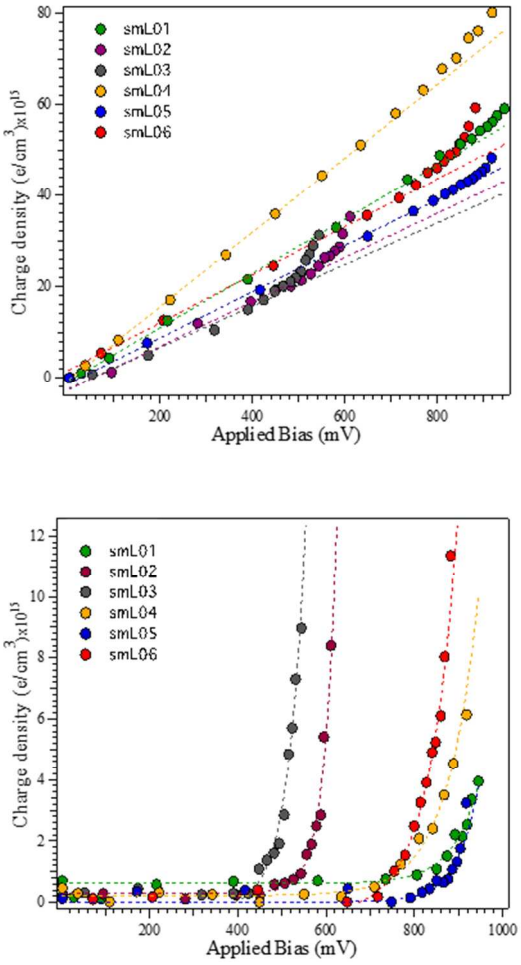

Fig. 5 up) Total charge density at the solar cell under different light bias (solar cell voltage at different light illumination intensities) and down) Charge density after subtracting the geometrical capacitance (Eq. 2).

Following the CE measurements, we carried out transient photovoltage[2022] (TPV) measurements in order to determine and compare the different charge lifetimes for the materials with points close to the V_{oc} at 1 sun conditions (in applied bias). These experimental points were fitted to a power-law exponential decay.

It can be seen from Fig. 6 that all of the compounds had similar decay orders, which indicates that in all cases the behaviour is far from second order. A recombination order close to 2 would indicate that the measured kinetics correspond mainly to a non-geminate bimolecular charge recombination reaction. The devices with **smL02** and **smL03** clearly had the fastest recombination rates as the number of thienylenevinylenes on both sides of the molecular backbone increases. In particular, the non-geminate recombination is higher due to the location of the HOMO.

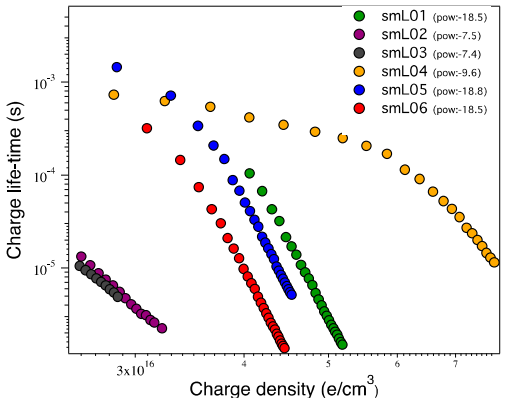

Fig. 6 Charge lifetimes of all organic solar cells measured in Fig. 2 under the same light bias as in Fig. 4. The power law decay order after fitting the linear part of each curve is shown in parentheses.

Finally, charge mobility measurements (Fig. 7) were carried out by obtaining an IV curve for hole-only devices for each **smL** molecule. The diode was forced to work under space-charge-limited current (SCLC) conditions.

The plots were fitted to the Murgatroyd equation (Eq. 3), which includes the effects of electric field and charge defects through the *Poole–Frenkle* factor.

Equation 3 $$J_{SCLC} = \frac{9}{8}\varepsilon\mu\frac{V_{eff}^2}{d^3}\exp\left(\frac{0.89\beta\sqrt{V_{eff}}}{\sqrt{d}}\right)$$

Where ε is the permittivity of the medium, μ is the mobility, d the film thickness, β is the Poole–Frenkle factor and V_{eff} is the voltage ($V_{eff} = V_{oc} - V_{bi}$). The mobility results are listed in Table 3. Plots of the mobility results can be found in the SI.

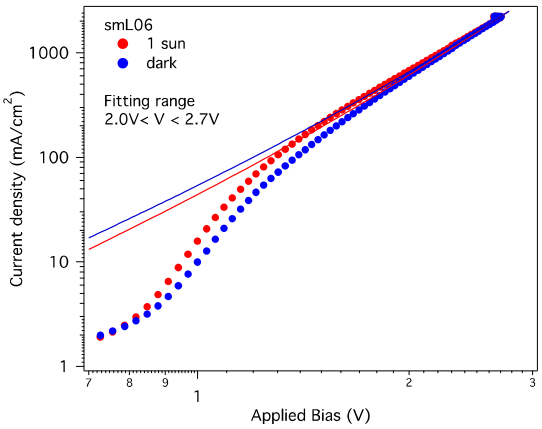

Fig. 7 IV curves for a hole-only device of **smL06:PC$_{71}$BM** bulk-heterojunction 75 nm thick film under sun simulated irradiation (100 mW cm^{-2}) and in the dark. The corresponding fitting was performed in the voltage range in the figure legend.

Table 3 Hole mobility and *Poole–Frenkle* values for all **smL**:**PC$_{71}$BM** organic solar cells

Device	h^+ mobility (Vcm^{-2}s^{-1})	β (Poole–Frenkle factor)
smL01	$1.2 \pm 0.7\times10^{-6}$	6.04×10^{-3}
smL02	$1.1 \pm 0.2\times10^{-5}$	3.94×10^{-3}
smL03	$2.8 \pm 0.8\times10^{-5}$	4.33×10^{-3}
smL04	$5.9 \pm 3.1\times10^{-7}$	9.13×10^{-3}
smL05	$1.8 \pm 0.9\times10^{-4}$	1.07×10^{-3}
smL06	$1.4 \pm 0.2\times10^{-5}$	4.75×10^{-3}

The hole mobility results show a range of three orders of magnitude. Taking **smL01** as the reference, **smL02** and **smL03** show a marked increase in mobility (from $\times10^{-6}$ to $\times10^{-5}$ Vcm^{-2}s^{-1}) as the number of thiophene groups and their respective alkyl chains increase. The effect of the alkyl chains is reflected in the results for **smL04**, where the absence of two of the alkyl chains retarded the hole mobility by one order of magnitude (from $\times10^{-6}$ to $\times10^{-7}$ Vcm^{-2}s^{-1}). Moreover, the mobility values for **smL05** and **smL06** are one and two orders of magnitude higher than for **smL01**. The highest hole mobility was obtained for **smL05** and this evidences the remarkable contribution of alkyl chains to the hole mobility.

Experimental

Synthesis and characterization

Synthesis of diethyl 3-hexylthienylmethylphosphonate (3). $NaBH_4$ (0.43 g, 11.4 mmol) was added portionwise to a solution of aldehyde **1** (1.12 g, 5.7 mmol) in 1:1 CH_2Cl_2/methanol (60 mL). The mixture was stirred for 45 min, diluted with CH_2Cl_2 and washed with water. After extraction with CH_2Cl_2, the organic phase was dried over $MgSO_4$ and the solvent was evaporated to give alcohol **2** in quantitative yield. The product was pure by TLC and ^{1}H NMR and it was used in the next step without further purification.

$ZnBr_2$ (1.5 g, 6.7 mmol) was added to a solution of the alcohol **2** (1.11 g, 5.6 mmol) and triethylphosphite (5 mL, 28 mmol) at room temperature. The mixture was stirred for 20 h under argon. After consumption of the starting material (monitored by TLC), the reaction was poured over crushed ice containing conc. HCl, extracted with $CHCl_3$ and the organic layer was dried over $MgSO_4$. The solvent was removed under vacuum and the solid was purified by column chromatography (silica-flash, hexane:ethyl acetate 3:2). Compound **3** was obtained as colourless oil in 84% yield (1.5 g, 4.7 mmol).

^{1}H-NMR (400 MHz, $CDCl_3$): δ/ppm: 7.13–7.11 (m, 1H), 6.85–6.84 (m, 1H), 4.10–4.03 (m, 4H), 3.31 (d, 2H, J = 20.8 Hz), 2.58–2.53 (m, 2H), 1.58–1.53 (m, 2H), 1.30–1.21 (m, 12H), 0.90–0.87 (m, 3H); ^{13}C-NMR (100 MHz, $CDCl_3$): δ/ppm: 140.8, 140.7, 128.6, 128.5, 125.7, 125.6, 123.2, 123.1, 62.4, 62.3, 31.8, 30.5, 30.4, 29.2, 28.4, 28.3, 27.0, 25.5, 22.6, 16.4, 16.3, 14.1; FT-IR (ATR): υ/cm^{-1}: 2928, 2858, 1254, 1053, 1022, 960, 725.

Synthesis of 4.

In a round-bottomed flask, under an argon atmosphere, diethyl 3-hexylthienylmethylphosphonate (**3**) (100 mg, 0.314 mmol) and 3,4-ethylenedioxythiophenedicarboxyaldehyde (28.3 mg, 0.143 mmol) were dissolved in dry THF (10 mL). The mixture was cooled to –78 ºC and *t*-BuOK (48.1 mg, 0.43 mmol) was added. The mixture was stirred for 2 h at the same temperature. The yellow solution was extracted three times with diethyl ether. The organic phase was dried over $MgSO_4$, concentrated in vacuum and the resulting solid was purified by column chromatography (flash silica, hexane:CH_2Cl_2 8:2). Compound **4** was obtained as a yellow solid in 36% yield (27 mg, 0.051 mmol).

^{1}H-NMR (400 MHz, $CDCl_3$): δ/ppm: 7.07 (d, 2H, J = 4.8 Hz), 6.96 d, 2H, J = 15.6 Hz), 6.90 (d, 2H, J = 15.6 Hz), 6.84 (d, 2H, J = 4.8 Hz), 4.31 (s, 4H), 2.66 (t, 4H, J = 7.6 Hz), 1.60 (m, 4H), 1.34 (m, 12H), 0.91 (m, 6H); ^{13}C-NMR (100 MHz, $CDCl_3$) δ/ppm: 140.6, 139.3, 136.6, 129.8, 122.6, 118.0, 116.8, 115.3, 64.9, 31.7, 30.9, 29.0, 28.4, 22.6, 14.2; UV-vis (CH_2Cl_2) λ_{max}/nm (log ε): 436 (4.33), 328 (4.07); FT-IR (ATR): υ/cm^{-1}: 2923, 2854, 1442, 1362, 1080, 933; MS (*m*/*z*) (MALDI-TOF): calculated for $C_{30}H_{38}O_2S_3$: 526.20; found 526.70 (M^+).

Synthesis of 5a.

In a round-bottomed flask, under an argon atmosphere, $POCl_3$ (63 mg, 0.41 mmol) was added to a solution of **4** (48 mg, 0.091 mmol) and DMF (42 mg, 0.57 mmol) in dry dichloroethane (10 mL). The mixture was stirred overnight at room temperature. 1 M sodium acetate was added to neutrality and the mixture was stirred vigorously for 1 h. The solution was extracted with dichloromethane and the organic phase was dried over $MgSO_4$. After evaporation of the solvent, the product was purified by column chromatography (flash silica, hexane: CH_2Cl_2 1:1) to give compound **5a** as a red solid in 73% yield (39 mg, 0.07 mmol).

^{1}H-NMR (400 MHz, $CDCl_3$): δ/ppm: 9.80 (s, 2H), 7.51 (s, 2H), 7.15 (d, 2H, J = 15.6 Hz), 6.97 (d, 2H, J = 15.6 Hz), 4.35 (s, 4H), 2.68 (m, 4H), 1.63 (m, 4H), 1.35 (m, 12H), 0.92 (m, 6H); ^{13}C-NMR (100 MHz, $CDCl_3$) δ/ppm: 182.4, 147.0, 141.8,

140.9, 139.4, 138.9, 121.0, 117.5, 116.5, 65.0, 31.6, 30.5, 28.9, 28.3, 22.6, 14.1; UV-Vis (CH_2Cl_2) λ_{max}/nm (log ε): 479 (4.6), 382 (4.2); FT-IR (KBr) υ/cm^{-1}: 2928, 2850, 1651, 1601, 1431, 1362, 1281, 1080, 930, 667; MS (*m*/*z*) (MALDI-TOF): calculated for $C_{32}H_{38}O_4S_3$: 582.19; found 582.30 (M^+).

Synthesis of smL04.

In a round-bottomed flask, under an argon atmosphere, 3 drops of Et_3N were added to a solution of malononitrile (17 mg, 0.25 mmol) and bis-aldehyde **5a** (49 mg, 0.084 mmol) in $CHCl_3$ (10 mL). The reaction mixture was stirred at room temperature for 5 h and washed with brine. The organic phase was dried over $MgSO_4$ and the solvent was removed by evaporation under reduced pressure. After purification by column chromatography (silica gel, n-hexane:CH_2Cl_2 1:1), compound **smL04** was obtained in 70% yield (40 mg, 0.06 mmol).

^{1}H-NMR (400 MHz, $CDCl_3$): δ/ppm: 7.66 (s, 2H), 7.43 (s, 2H), 7.21 (d, 2H, *J* = 15.6 Hz), 6.99 (d, 2H, *J* = 15. 6 Hz), 4.38 (s, 4H), 2.67 (t, 4H, *J* = 7.6 Hz), 1.56 (m, 4H), 1.34 (m, 12H), 0.91 (m, 6H); ^{13}C-NMR (100 MHz, $CDCl_3$): δ/ppm: 149.9, 149.5, 142.6, 141.8, 141.6, 132.1, 122.9, 117.7, 117.2, 114.7, 113.8, 75.0, 65.0, 31.5, 30.4, 28.9, 28.0, 22.6, 14.1; UV-Vis (CH_2Cl_2) λ_{max}/nm (log ε): 611 (4.9), 362 (4.1), 327 (4.2); FT-IR (KBr) υ/cm^{-1}: 2930, 2860, 2210, 1560, 1410, 1280, 1080, 930; MS (*m*/*z*) (MALDI-TOF): calculated for $C_{38}H_{38}N_4O_2S_3$: 678.22; found 678.35 (M^+).

General procedure for the synthesis of smL05 and smL06.

The corresponding bis-aldehyde, **5a** or **5b**, was dissolved in dry $CHCl_3$. 3 drops of piperidine and then 3-ethylrhodanine were added and the resulting solution was heated under reflux for 12 h under argon. The reaction mixture was extracted with CH_2Cl_2, washed with brine and dried over $MgSO_4$. After removal of solvent, the product was purified by column chromatography (silica gel, n-hexane:CH_2Cl_2 1:1).

Synthesis of smL06: From 0.07 mmol of **5a** and 0.21 mmol of 3-ethylrhodanine. **smL06** was obtained as a blue solid in 69% yield (41 mg, 0.047 mmol).

^{1}H-NMR (400 MHz, $CDCl_3$) δ/ppm: 7.77 (s, 2H), 7.16 (s, 2H), 7.10 (d, 2H, *J* = 15.6 Hz), 6.95 (d, 2H, *J* = 15.6 Hz), 4.39 (s, 4H), 4.19 (q, 4H, *J* = 6.8 Hz), 2.66 (t, 4H, *J* = 7.6 Hz), 1.63–1.59 (m, 4H), 1.35–1.20 (m, 18H), 0.92 (m, 6H); ^{13}C-NMR (100 MHz, $CDCl_3$) δ/ppm: 192.1, 167.3, 146.1, 142.8, 140.8, 137.3, 134.8, 125.1, 120.1, 120.0, 117.2, 116.9, 65.0, 39.9, 31.6, 30.6, 28.9, 28.2, 22.6, 14.1, 12.3; UV-Vis (CH_2Cl_2) λmax/nm (log ε): 622 (5.0), 387 (4.6), 327 (4.6); FT-IR (KBr) υ/cm^{-1}: 2930, 2860, 1700, 1570, 1420, 1230, 1120, 879; MS (*m*/*z*) (MALDI-TOF): calculated for $C_{42}H_{48}N_2O_4S_7$: 868.17; found 868.39 (M^+).

Synthesis of smL05: From 0.05 mmol of **5b** and 0.14 mmol of 3-ethylrhodanine. **smL05** was obtained as a blue solid in 62% yield (30 mg, 0.03 mmol).

^{1}H-NMR (400 MHz, $CDCl_3$) δ/ppm: 7.90 (s, 2H), 7.12 (d, 2H, *J* = 15.6 Hz), 6.98 (d, 2H, *J* = 15.6 Hz), 4.40 (s, 4H), 4.20 (q, 4H, *J* = 6.8 Hz), 2.71 (t, 4H, *J* = 7.6 Hz), 2.62 (t, 4H, *J* = 7.6 Hz), 1.52 (m, 8H), 1.42–1.29 (m, 30H), 0.93–0.91 (m, 12H); ^{13}C-NMR (100 MHz, $CDCl_3$) δ/ppm: 192.4, 167.5, 150.7, 145.9, 141.9, 140.9, 130.7, 123.8, 120.0, 119.0, 117.6, 117.0, 65.02, 39.9, 31.8, 31.6, 31.5, 31.0, 29.4, 29.3, 27.6, 27.0, 22.6, 14.2, 14.1, 12.4; UV-vis (CH_2Cl_2) λ_{max}/nm (log ε): 632 (4.9), 393 (4.5), 330 (4.6); FT-IR (KBr) υ/cm^{-1}: 2920, 2850, 1700, 1570, 1320, 1230, 1130, 1080, 879; MS (*m*/*z*) (MALDI-TOF): calculated for $C_{54}H_{72}N_2O_4S_7$: 1036.35; found 1036.52 (M^+).

Device fabrication and characterization

Pre-patterned Indium Tin Oxide (ITO) 5 Ohm/square sodalime glass substrates were rinsed with acetone to remove the residual photoresist layer. The substrates were then placed in a Teflon holder and sequentially sonicated in acetone (1 × 10 min) and isopropanol (2 × 10 min) and finally dried under a nitrogen flow. The ITO substrates were ozone-treated in a UV-ozone cleaner for 30 min in an ambient atmosphere, and subsequently coated in air with a layer of a filtered (0.45 μm, cellulose acetate) solution of poly(3,4-ethylenedioxythiophene): poly(styrenesulphonate) (4500 rpm 30 seconds followed by 3500 rpm 30 seconds). The PEDOT:PSS film was dried at 120 ºC under an inert atmosphere for 15 min. Active layers were spin-coated (8000 rpm) in air over the PEDOT:PSS layer from a 20 mg/mL (total concentration) solution of donor derivative and $PC_{71}BM$ with a 1:2 ratio by weight. The solvent annealing step was carried out immediately after deposition of the active layer by exposing the films to a saturated vapour atmosphere of dichloromethane in a controlled volume closed vessel. The vessel (100 mL) was filled with 10 mL of CH_2Cl_2 and left sealed for 5 min prior to the SVA step to ensure saturation of the atmosphere. The substrates were exposed to the solvent vapours from one to several minutes by placing them in the solvent vessel.

The cathode layer was deposited by thermal evaporation in an ultra-high vacuum chamber ($1\cdot 10^{-6}$ mbar). Metals were evaporated through a shadow mask leading to devices with an area of 9 mm^2. LiF (0.6 nm) and Al (80 nm) were deposited at a rate of 0.1 Å/s and 0.5–1 Å/s, respectively. Following fabrication, the films were maintained under a nitrogen atmosphere and stored in the dark until used. In the cases of hole-only and electron-only devices the solar cells were prepared as explained above, but for hole-only devices the structure was ITO/PEDOT:PSS/donor:$PC_{71}BM$/Au and for electron-only devices the structure was ITO/ZnOnp/donor:$PC_{71}BM$/Al. All device efficiency values correspond to masked devices with an active area of 9 mm^2.

The UV-Vis absorption spectra of films were measured using a Shimadzu UV-1700 spectrophotometer. The J-V characteristics of the devices were measured using a Sun 2000 Solar Simulator (150 W, ABET Technologies). The illumination intensity was measured to be 100 mW cm^{-2} with a calibrated silicon photodiode (NREL). The appropriate filters were utilized to faithfully simulate the AM 1.5G spectrum. The applied potential and cell current were measured with a Keithley 2400 digital source meter. The current-to-voltage (IV) curve was plotted automatically with in-house Labview© software. The thickness of the films was measured with a stylus profilometer (Ambios Tech. XP-1) from a scratch made in the middle of the film.

Conclusions

In conclusion, we have designed and synthesized a series of organic semiconductor molecules based on the EDOT unit as a donor moiety for small molecule solution-processed bulk heterojunction solar cells. Efficiencies of 4.9% were achieved under standard simulated illumination conditions. The **smL01** molecule has the highest light harvesting efficiency (65%), although it was demonstrated that all device performances were mainly limited by lower mobility, which limited the fabrication of the solar cells to very thin active layers. An increase in the number of thiophene units and the use of alkyl chains broadens the absorption spectra to the red and allows higher fill factors (FF) in the solar cells, as observed for **smL02** and **smL03**. However, an increase in charge recombination was also observed in these cases. In the TPV measurements both **smL02** and **smL03** present higher recombination rates compared to the other members of the smL family; thus, it seems that thiophene units increase the hole mobility but also increase charge recombination. Finally, **smL06** presented the highest efficiency and an outstanding photocurrent of 12 mA cm^{-2}. The main reason for this result is the higher internal conversion efficiency of the device, as reflected by the fact that this compound has the highest IPCE value despite not having the highest LHE and not having the best hole mobility values.

Acknowledgements

We would like to thank MINECO for funding projects CTQ2013-47183-R and CTQ2013-48252-P. EP thanks the support through Severo Ochoa Excellence Accreditation 2014-2018(SEV-2013-0319). RD thanks the Ministerio de Educación, Cultura y Deporte of Spain for an FPU grant and BP thanks MINECO for an FPI grant.

Notes and references

[a] Institute of Chemical Research of Catalonia (ICIQ), Avinguda del Països Catalans 16, 43007 Tarragona, Spain. Fax: +34 977 920 823; Tel: +34 977 920 200; E-mail: epalomares@iciq.es
[b] Institute for Nanoscience, Nanotechnology and Molecular Materials (INAMOL). University of Castilla-la Mancha, Campus de la Fábrica. 45071. Toledo, Spain. E-mail: Fernando.Langa@uclm.es
[c] Catalan Institution for Research and Advanced Studies (ICREA), Passeig de Lluis Companys 23, 08010 Barcelona, Spain
[+] These authors contributed equally to this work.

†Electronic Supplementary Information (ESI) available. See DOI: 10.1039/b000000x/

References

1 B. Kan, Q. Zhang, M. Li, X. Wan, W. Ni, G. Long, Y. Wang, X. Yang, H. Feng and Y. Chen, *J. Mater. Chem.*, 2014, **136**, 15529.
2 J. Peet, J. Y. Kim, N. E. Coates, W. L. Ma, D. Moses, A. J. Heeger and G. C. Bazan, *Nat. Mater.*, 2007, **6**, 497.
3 G. C. Welch, L. A. Perez, C. V. Hoven, Y. Zhang, X.-D. Dang, A. Sharenko, M. F. Toney, E. J. Kramer, T. Q. Nguyen and G. C. Bazan, *J. Mater. Chem.*, 2011, **21**, 12700.
4 A. K. K. Kyaw, D. H. Wang, V. Gupta, J. Zhang, S. Chand, G. C. Bazan and A. J. Heeger, *Adv. Mater.*, 2013, **25**, 2397.
5 M. Chandrasekharam, M. Anil Reddy, K. Ganesh, G. D. Sharma, S. Prakash Singh and J. Laxmikanth Rao, *Org. Electron.*, 2014, **15**, 2116.
6 H. Bürckstümmer, N. M. Kronenberg, M. Gsänger, M. Stolte, K. Meerholz and F. Würthner, *J. Mater. Chem.*, 2010, **20**, 240.
7 H. Bürckstümmer, E. V. Tulyakova, M. Deppisch, M. R. Lenze, N. M. Kronenberg, M. Gsänger, M. Stolte, K. Meerholz and F. Würthner, *Angew. Chem. Int. Ed.*, 2011, **50**, 11628.
8 N. M. Kronenberg, V. Steinmann, H. Bürckstümmer, J. Hwang, D. Hertel, F. Würthner and K. Meerholz, *Adv. Mater.*, 2010, **22**, 4193.
9 S.-W. Chiu, L.-Y. Lin, H.-W. Lin, Y.-H. Chen, Z.-Y. Huang, Y.-T. Lin, F. Lin, Y.-H. Liu and K.-T. Wong, *Chem. Commun.*, 2012, **48**, 1857.
10 Y.-H. Chen, L.-Y. Lin, C.-W. Lu, F. Lin, Z.-Y. Huang, H.-W. Lin, P.-H. Wang, Y.-H. Liu, K.-T. Wong, J. Wen, D. J. Miller and S. B. Darling, *J. Am. Chem. Soc.*, 2012, **134**, 13616.
11. N. F. Montcada, B. Pelado, A. Viterisi, J. Albero, J. Coro, P. de la Cruz, F. Langa and E. Palomares, *Org. Electron.*, 2013, **14**, 2826.
12. H. Bürckstümmer, N. M. Kronenber, M. Gsänger, M. Stolte, K. Meerholz and F. Würthner, *J. Mater. Chem.*, 2010, **20**, 240.
13. W. Wu, Y. Liu and D. Zhu, *Chem. Soc. Rev.*, 2010, **39**, 1489.
14. B. Kim, X. Ma, C. Chen, Y. Ie, E. W. Coir, H. Hashemi, Y. Aso, P. F. Green, J. Kieffer and J. Kim, *Adv. Funct. Mater.*, 2013, **23**, 439.
15. Y. Li, *Acc. Chem. Res.*, 2011, **45**, 723.
16. F. Langa et al. Manuscript in preparation.
17. This value for E_{LUMO} is rough as the exciton binding energy is neglected. See J.L. Bredas, *Mater. Horiz.* 2014, **1**, 17.
18. G. C. Welch, L. A. Perez, C. V. Hoven, Y. Zhamg, X. D. Dang, A. Sharenko, M. F. Toney, E. J. Kramoer, T. Q. Nguyen and G. C. Banzan, *J. Mater. Chem.*, 2011, **21**, 12700.
19. P. M. Beaujuge and J. M. J. Fréchet, *J. Am. Chem. Soc.*, 2011, **133**, 20009.
20. A. Guerrero, N. F. Montcada, J. Ajuria, I. Etxebarria, R. Pacios, G. Garcia-Belmonte and E. Palomares, *J. Mater. Chem. A*, 2013, **1**, 12345.
21. A. Sánchez-Díaz, L. Burtone, M. Riede and E. Palomares, *J. Phys. Chem. C*, 2012, **116**, 16384.
22. A. Sánchez-Díaz, R. Pacios, U. Muñecas, T. Torres and E. Palomares, *Org. Electron.*, 2011, **12**, 329.